Developmental Biology 394 (2014) 197–205

Contents lists available at ScienceDirect

Developmental Biology

journal homepage: www.elsevier.com/locate/developmentalbiology

Short Communication

Local and global dynamics of the basement membrane during branching morphogenesis require protease activity and actomyosin contractility

Jill S. Harunaga, Andrew D. Doyle, Kenneth M. Yamada*

Cell Biology Section, Laboratory of Cell and Developmental Biology, National Institute of Dental and Craniofacial Research, National Institutes of Health, 30 Convent Drive, Building 30, Room 403, Bethesda, MD 20892, USA

ARTICLE INFO

Article history:
Received 22 May 2014
Received in revised form
14 August 2014
Accepted 16 August 2014
Available online 23 August 2014

Keywords:
Basement membrane
Matrix dynamics
Branching morphogenesis
Proteases
Myosin II

ABSTRACT

Many epithelial tissues expand rapidly during embryonic development while remaining surrounded by a basement membrane. Remodeling of the basement membrane is assumed to occur during branching morphogenesis to accommodate epithelial growth, but how such remodeling occurs is not yet clear. We report that the basement membrane is highly dynamic during branching of the salivary gland, exhibiting both local and global remodeling. At the tip of the epithelial end bud, the basement membrane becomes perforated by hundreds of well-defined microscopic holes at regions of rapid expansion. Locally, this results in a distensible, mesh-like basement membrane for controlled epithelial expansion while maintaining tissue integrity. Globally, the basement membrane translocates rearward as a whole, accumulating around the forming secondary ducts, helping to stabilize them during branching. Both local and global dynamics of the basement membrane require protease and myosin II activity. Our findings suggest that the basement membrane is rendered distensible by proteolytic degradation to allow it to be moved and remodeled by cells through actomyosin contractility to support branching morphogenesis.

Published by Elsevier Inc.

Introduction

During embryonic development, expanding epithelial tissues generally remain tightly associated with a basement membrane (BM), a dense, sheet-like type of specialized extracellular matrix composed primarily of laminin, collagen IV, nidogen, and the heparan sulfate proteoglycan, perlecan. A network of laminin self-assembles via cell surface interactions to initiate the formation of a BM (Yurchenco, 2011; McKee et al., 2007). Collagen IV then polymerizes to form a second covalently crosslinked network, which provides the bulk of the mechanical strength (Poschl et al., 2004); the two networks are linked together by nidogen and perlecan (Kelley et al., 2014; Hohenester and Yurchenco, 2013). The morphology and composition of the BM varies between tissue types, and it can also change with age, e.g., the BM of the cornea thickens and increases in stiffness over the course of adult human aging (Halfter et al., 2013; Candiello et al., 2010). These findings suggest that the BM is not a static structure and can change throughout the lifetime of the organism.

Rapid expansion of the epithelium occurs during certain stages of branching morphogenesis of lung, submandibular salivary gland (SMG), kidney, mammary gland, and other organs. This process of epithelial bud expansion and branching by cleft formation is a key developmental process to maximize organ epithelial surface area for secretion and adsorption (Patel et al., 2006). Although the morphology of these embryonic organs differ (Fig. 1A), all such epithelia are encapsulated by a BM that separates the epithelium from the surrounding mesenchyme (Patel et al., 2006; Kim and Nelson, 2012; Andrew and Ewald, 2010). BMs play multiple important roles in morphogenesis, with functions that include providing tissue structural support and boundaries, mediating growth factor signaling, and providing polarity cues (Rozario and DeSimone, 2010). Because the BM provides such important cues while the epithelium expands rapidly during development, the BM must be rapidly remodeled to accommodate the expanding tissue while continuing to surround the epithelium. While many laboratories have investigated how cells invade through a BM, particularly in pathological processes such as cancer metastasis (Rowe and Weiss, 2009), the fundamental question of how normal embryonic epithelia can expand rapidly while remaining encapsulated by a BM is poorly understood.

Recent studies in *Drosophila* egg chamber, mammary and salivary glands have shown that cells can orient, translocate, and accumulate the surrounding BM to help shape the architecture of the tissue (Daley and Yamada, 2013; Haigo and Bilder, 2011; Fata et al., 2004; Larsen et al., 2006; Wang et al., 2013). Proteolytic remodeling of the BM is required for branching morphogenesis in

* Corresponding author.
E-mail address: kenneth.yamada@nih.gov (K.M. Yamada).

http://dx.doi.org/10.1016/j.ydbio.2014.08.014
0012-1606/Published by Elsevier Inc.

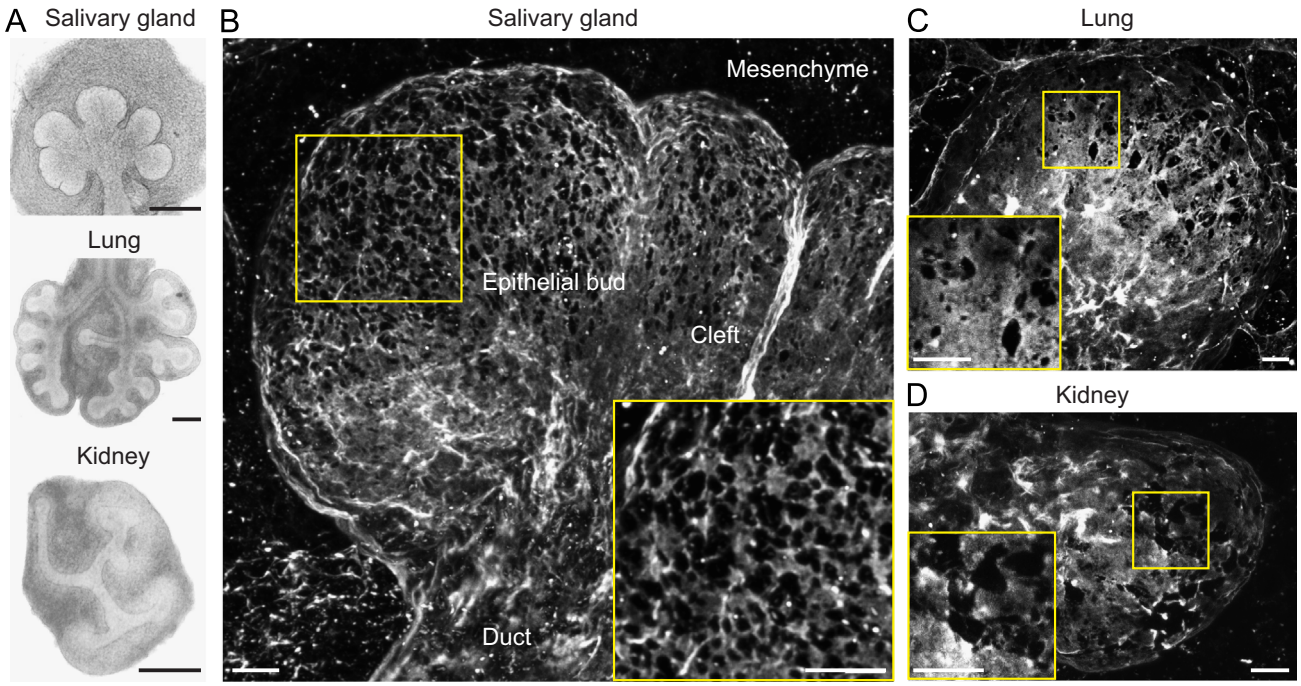

Fig. 1. Micro-perforated basement membranes are present in multiple embryonic organs. (A) Brightfield images of an E13 SMG, E11 lung, and E11 kidney show the differences in morphology among developing branched organs; scale bars: 200 μm. (B) Maximum-intensity projection of an E13 SMG immunostained for collagen IV with labels indicating an epithelial bud with a developing cleft and its duct, surrounded by mesenchyme. Maximum projection images of confocal slices of E11 lung (C) and kidney (D) immunostained for laminin. Scale bars: 20 μm and 10 μm for the insets, respectively.

several organs (Wessells and Cohen, 1968; Banerjee et al., 1977; Nakanishi et al., 1986). Specifically, matrix metalloproteases are necessary for lung, salivary and mammary gland branching, allowing outgrowth (Fata et al., 2004) and growth factor release (Rebustini et al., 2009) that contribute to branching. During chick development, prior to gastrulation and EMT invasion, the BM moves along with the epiblast cells in primitive streak formation (Zamir et al., 2008), suggesting either that the cells and matrix move together as a tissue, or that the cells tow their underlying matrix with them as the migrate. Normal cells can also traverse the BM under certain circumstances. During *Caenorhabditis elegans* uterine-vulva formation, a break in the BM is initiated by anchor invadopodia, and this gap is widened by cell-mediated mechanical displacement and sliding of the BM (Kelley et al., 2014; Ihara et al., 2011; Hagedorn et al., 2013). Leukocytes also must cross BMs to enter and exit lymph vessels; they do so through preexisting holes in the BM that become mechanically dilated as the cell squeezes through (Pflicke and Sixt, 2009). In the present study, we report that the BM surrounding branching organs is highly dynamic, exhibiting both local and global remodeling via protease activity and actomyosin contractility, while still surrounding an intact epithelial compartment.

Materials and methods

Dissection

SMGs were dissected from the following mouse strains at embryonic day 12.5 (E12.5; E0 is defined as the day of conception with a vaginal plug): wild-type ICR (Harlan), homozygous eGFP-myosin IIA knock-in transgenic (B6, 129, BALB) (Zhang et al., 2012) or homozygous eGFP-myosin IIB knock-in transgenic (C57BL6 and 129Sv, MMRRC, ID# 37053) (Fischer et al., 2009). Myosin II knock-in mice were generated in the laboratory of Robert Adelstein (NHLBI) and bred in-house. All mice were housed, bred, and euthanized according to an approved NIDCR animal study protocol.

Live imaging

Collagen IV antibody was labeled as previously described (Hsu et al., 2013). Mouse SMGs were dissected and cultured on 0.2 μm filters overnight; the filter and glands were inverted so that the glands faced the cover glass of a MatTek dish; the filter was secured to the glass with vacuum grease along the periphery of the filter. Glands were cultured in media plus OxyFluor (Oxyrase) and 5 μg/ml DyLight-649-labeled collagen IV antibody for 2–5 h. Live-organ imaging was performed using a CSU-Z1 spinning disc confocal (Yokogawa) on an Axiovert 200 M microscope (Zeiss) with either a EM-CCD camera (Photometrics) or a sCMOS camera (Hamamatsu) using a 40X C-Apochromat water objective (NA 1.2) or a 63X Plan-Apochromat oil objective (NA 1.4). The lasers, stage, chamber, and software were described previously (Hsu et al., 2013). Laser power settings were set to 15% for 488 nm and 10% for 647 nm. Exposure times were 500–800 ms for each channel. Glands were imaged for 20 min to 12 h, and intervals varied between 5 s to 10 min depending on the experiment.

For photo-bleaching of the BM, an iLAS FRAP module (Roper Scientific Europe) was used together with a 50 mW 405 nm diode laser (CrystaLaser) on the spinning disc confocal microscope. A 7×60 pixel box was drawn parallel to the tip of the bud and bleached at 55% power for 3 s.

See Supplementary material for more detailed methods.

Results and discussion

The basement membrane surrounding several embryonic branched organs becomes transiently perforated

During branching of the lung, mammary gland, and SMG, the BM is known to become thinner or display increased remodeling at the tips of expanding epithelial buds compared to cleft and duct regions (Bernfield and Banerjee, 1982; Mollard and Dziadek, 1998;

Silberstein and Daniel, 1982), suggesting that BM at these sites might exhibit increased mechanical compliance or distensibility (Moore et al., 2005). To determine if the BM demonstrates local morphological differences consistent with this hypothesis, we examined the BM surrounding the end buds of SMG, lungs, and kidneys undergoing morphogenesis at stages of rapid expansion (Fig. 1A). We visualized the entire BM by creating maximum projection images from several confocal Z-sections (Fig. S1A) of organs immunostained for collagen IV and laminin. This revealed that the BM was not a uniform sheet, but was instead perforated by numerous microscopic holes (Fig. 1B–D). The micro-perforations, or holes, were most prominent at regions of the BM surrounding the tips of the expanding end buds and were absent from the cleft and duct areas where expansion was low and BM accumulates (Fig. 1B; Movie S1). Focusing on the E13.5 SMG, we find that the holes appeared to penetrate through the entire BM according to immunolocalization of three major constituents of BM (Fig. 2A), collagen IV, laminin, and perlecan (Yurchenco, 2011).

Presence of BM micro-perforations was associated with the developmental stage of the SMG with the highest epithelial expansion and outgrowth; they are not present at the single bud stage at E12 and eventually disappear at E15 when differentiation begins (Fig. S1B). We documented the appearance of perforations in the same gland (Fig. S1F), as well as a decrease in the number and sizes of the holes starting at E14 (Movie S2). We quantified the micro-perforations at their peak in E13.5 SMGs. The sizes of the holes varied enormously, with the cross-sectional area of a perforation ranging from 0.01 to 15 μm^2, though $>90\%$ of the perforations had areas $<5\ \mu m^2$; their overall average size was $1.6\ \mu m^2 \pm 2.1$ (SD). This area is substantially smaller than an epithelial cell (estimated as $\sim 25\ \mu m^2$ at the basal surface) and would keep motile epithelial cells (Hsu et al., 2013) compartmentalized from the mesenchyme. We found that the distribution of the perforations varied across the end bud (Fig. 2B); the highest density was near the tip (Fig. 2C) with a loss of 27% of the BM surface area to holes. The percent perforated area decreased dramatically closer to the equator of the bud by nearly 7-fold, as the number and size of the perforations decreased (Fig. 2D and E). The shape of the perforations in all four assay regions was the same: elongated perpendicular to the tip of the bud, with an axial ratio of 1.7 (Fig. 2F).

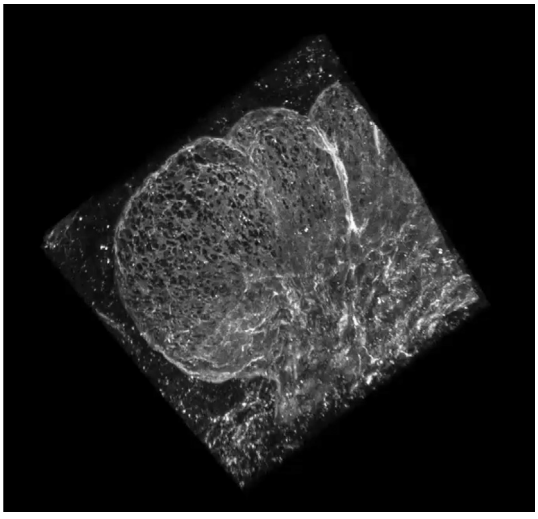

Movie 1. Three-dimensional rendering of E13 mouse submandibular salivary gland. Rotating image of half of an E13 salivary gland stained for collagen IV to display the perforations in the basement membrane. A video clip is available online. Supplementary material related to this article can be found online at http://dx.doi.org/10.1016/j.ydbio.2014.08.014.

The BM is highly dynamic during salivary gland development

To understand why the micro-perforations were distributed in a gradient over the end buds, we visualized remodeling of the BM in real time with a fluorescently labeled, non-perturbing collagen IV antibody and found the BM to be highly dynamic (Movies S2–S5). We observed both local matrix dynamics near the tip of the end buds involving dilation and contraction of the micro-perforations, as well as global dynamics involving translocation of the entire BM, rearward toward the duct while the bud expanded outward. We quantified the translocation by photobleaching a rectangular region of BM parallel to the tip of the bud and found that the BM translocated steadily and continuously over the end bud at 8 μm/h (Fig. 3A and C; Movie S3), with the long axis of the micro-perforations oriented longitudinally (Fig. 2F). The translocation slowed below the equator, and the BM matrix accumulated into dense aggregates (Fig. 1B, S1C; Movie S2). Previous research had indicated the importance of such extracellular matrix accumulation, especially collagen, in this region to stabilize the clefts and ducts, ultimately sculpting the tissue (Banerjee et al., 1977; Fukuda et al., 1988; Grobstein and Cohen, 1965). This BM accumulation occurred as the micro-perforations disappeared (Fig. 2B, region 4), indicating that the BM is actively translocated from the tip of the end bud to the center of the bud where it builds up, fills in the micro-perforations, and helps to shape and support the duct (Movie S2).

Extensive perforation of the BM is associated with increased distensibility and dynamics

The dramatic local distortions of the BM near the tips of the end buds (Fig. 3B and D; Movie S4) suggested that the high numbers of micro-perforations in this region locally alters the mechanical flexibility or distensibility of the BM. The area and shape of the micro-perforations fluctuated as rapidly as 4 μm^2 in less than 1 min (Fig. 3B and D). Although the tip of the bud was surrounded by a dynamic lattice-like BM, we have never observed significant fusion or stretching of the perforations such that epithelial cells would cross the BM. We found that the repetitive dilation and contraction of the micro-perforations was due to rapid physical distortion of the BM, rather than degradation or deposition of BM, since the fluctuations stopped within minutes of addition of the myosin II ATPase inhibitor, blebbistatin (Fig. 3D). The fact that the BM was so readily deformed indicated that the regions where the BM is abundantly perforated are highly compliant.

A complementary measure of BM distensibility was stretching of the BM itself. We tracked pairs of fiduciary marks on the BM surface and found that distensibility, defined as the maximum distance between two points subtracted from the minimum distance within a 20 min time period, was 2-fold higher near bud tips compared to the mid-bud (Fig. 3E; Movie S4). There was greater BM stretching in the tip region of the gland with larger, more numerous BM micro-perforations and high tissue expansion, consistent with enhanced local BM flexibility due to the perforations. The distensibility of the BM was dependent on actomyosin contraction, since local BM dynamics were inhibited by the addition of blebbistatin (Fig. 3D and E). Although it is not possible to exclude that there could be increased epithelial cell contraction of the BM near the bud equator, we observed no differences in myosin II localization or in the frequency of contractions (data not shown). Therefore, it seems most likely that the decreased flexibility of the BM is responsible for the decrease in area fluctuations of the micro-perforations and in our distensibility index at the equator of the bud compared to the tip region.

We also observed dynamic interactions of the epithelium with the BM by live imaging of SMGs from a GFP-labeled myosin II transgenic

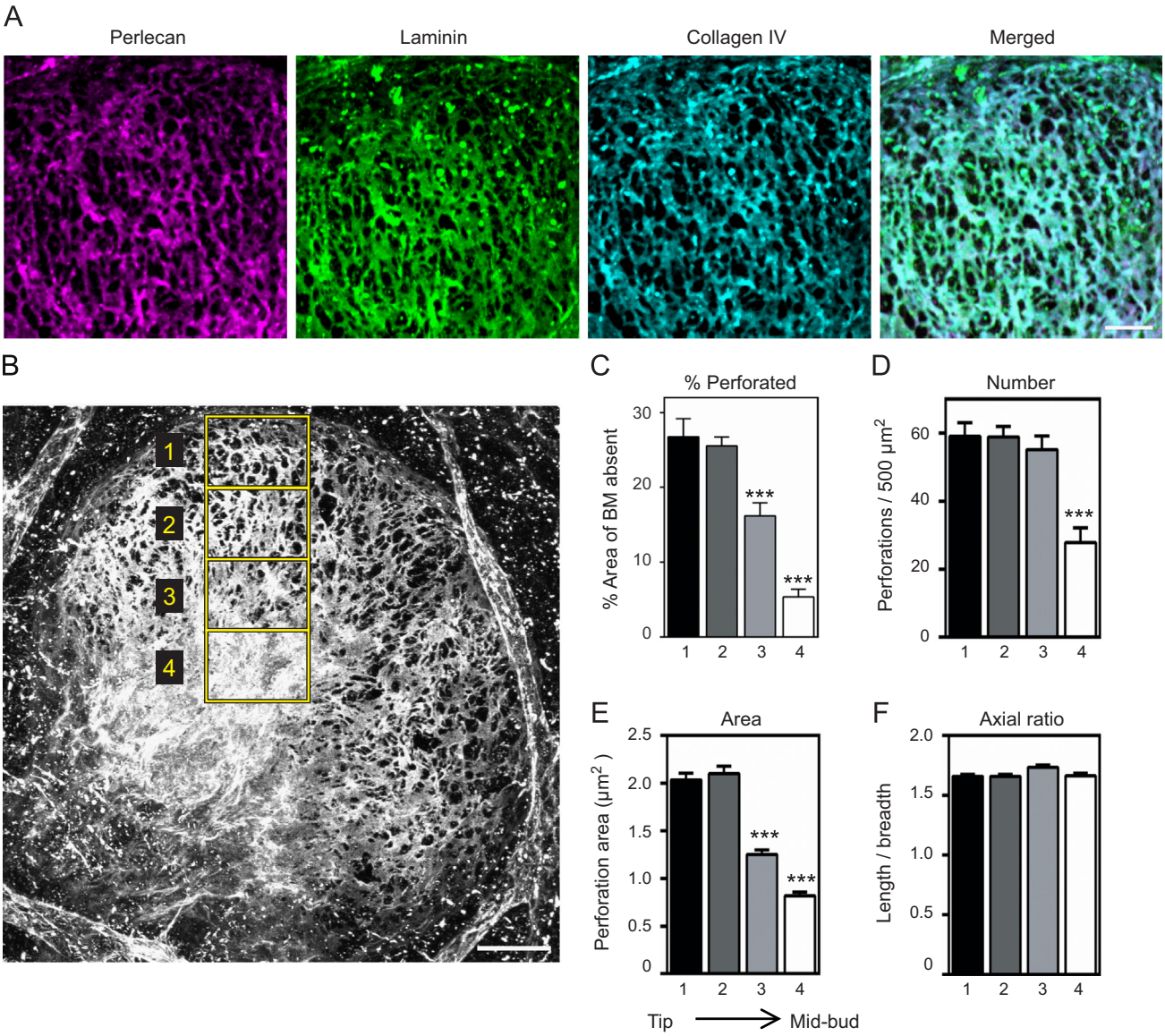

Fig. 2. Characterization of basement membrane perforations. (A) Maximum projection images of an E13 SMG stained for several BM components: perlecan (magenta), laminin (green), collagen IV (cyan), plus merged; scale bar: 10 μm. (B) Maximum projection of E13.5 SMG stained for collagen IV marked with 4 rectangular regions of equal size for comparative analysis, starting at the tip of the bud and ending at the center of the bud; scale bar: 20 μm. (C) Average percent surface area of BM absent (± SEM) based on region: region 1 = tip of the bud and 4 = center of the bud, as shown in 2B. (D) Average number of holes per 500 μm^2 area of BM, (E) average perforation areas, and (F) axial ratio of holes (± SEM) of each of the 4 different regions of the bud, $^{***}p < 0.001$.

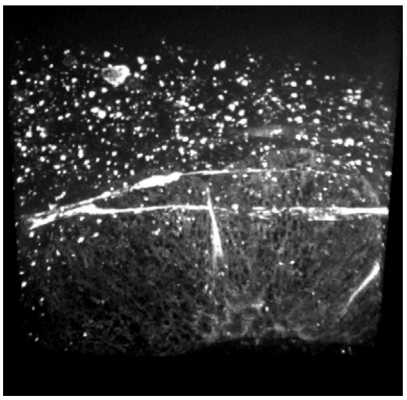

Movie 2. Three-dimensional rendering of 12 h timelapse movie of E13.5 mouse salivary gland. An E13.5 gland was imaged with a fluorescently labeled collagen IV antibody for 12 h. The perforations decrease in number and size over time, and the basement membrane translocates toward the duct, where it accumulates.

mouse with the fluorescently tagged collagen IV antibody. Basal epithelial cells frequently extended cell surface protrusions through and beyond the BM holes (Fig. 3F); these bleb-like protrusions could extend as far as 5 μm beyond the BM (Movie S5). These protrusions often extended repetitively through the same hole, confirming patency of the micro-perforations; furthermore, some protrusions expanded the perforations as they passed through (Movie S5). However, during these transient dilations, we did not observe accumulation of the BM around the periphery of the hole as seen in *C. elegans* anchor cell invasion (Hagedorn et al., 2013), suggesting that the BM around the SMG is distensible and that the holes are not enlarging for cell crossing. These membrane protrusions were observed only at the tips of end buds, protruding through BM perforations in both embryonic SMG and lung. These observations confirm classical electron microscopy studies investigating epithelial-mesenchymal inductive interactions that captured single images of a similar type of cell protrusion through a BM gap at the tip of end buds in embryonic branching organs, including lung,

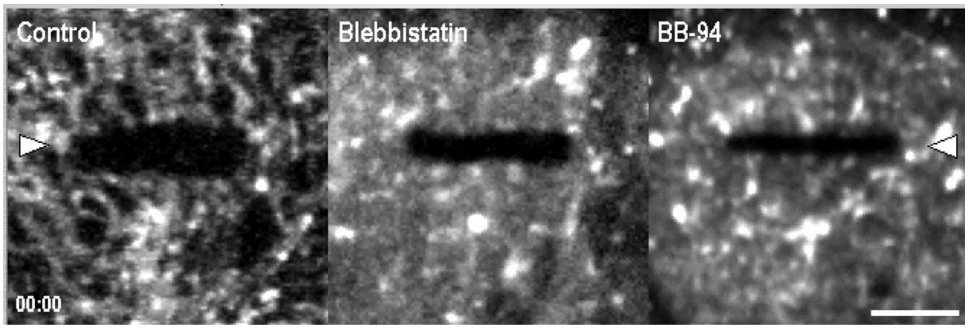

Movie 3. The basement membrane translocates rearward toward the duct. Maximum projection images of E13 salivary glands labeled with a fluorescently tagged collagen IV antibody showing the translocation of a bleached region of the basement membrane in glands with no treatment, 50 μM blebbistatin, or 5 μM BB-94. The white arrow heads indicate the starting point of the bleached regions. Scale bar: 10 μm.

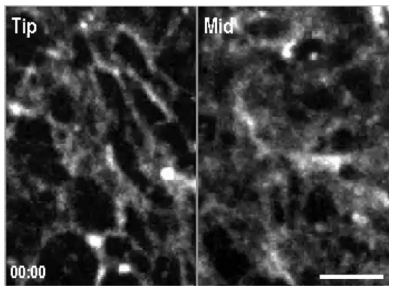

Movie 4. Basement membrane distensibility at the tip is higher than at the middle of the bud. Maximum projection of an E13 salivary gland imaged live with fluorescently labeled collagen IV antibody, showing a region of basement membrane near the tip of the bud (left) and a region near the middle of the bud (right). The basement membrane is highly dynamic at the tip of the bud, where the shape and size of the basement membrane perforations change rapidly, compared to the basement membrane located near to the middle of the bud. Time stamp is min: sec. Scale bar: 5 μm.

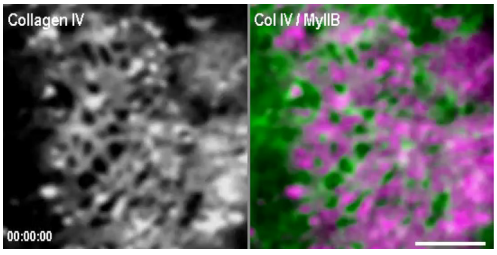

Movie 5. Submandibular salivary gland epithelial cells protrude through the basement membrane. Timelapse movie of the bottom of an eGFP-myosin IIB knock-in (green) E13 salivary gland bud imaged live with a fluorescently labeled collagen IV antibody (magenta). The basal epithelial cells protrude through holes in the basement membrane. Time stamp is h:min:s. Scale bar: 10 μm.

kidney and SMG (Bluemink et al., 1976; Cutler and Chaudhry, 1973; Lehtonen, 1975).

Protease activity is required for perforation formation and BM dynamics

A specific protease produced by the epithelium, MT2-MMP, had been previously implicated in releasing growth factors from the BM that promote epithelial proliferation and branching morphogenesis (Rebustini et al., 2009). We hypothesized that additional protease activity would be needed to form the BM perforations, which required the parallel loss of a collagen, a glycoprotein, and a proteoglycan. We tested this by treating the glands at E12.5, prior to BM perforation formation, with a variety of protease inhibitors. The most effective was the broadest protease inhibitor, batimastat (BB-94), which inhibits several MMPs (matrix metalloproteases) and two ADAMs (a disintegrin and metalloprotease). With this inhibitor, micro-perforations did not form (Fig. 4A and B), and branching was significantly inhibited. Treatment with a slightly less broad protease inhibitor of MMPs, GM6001, had similar effects, though to a lesser degree compared to glands treated with BB-94 (Fig. S1D). TIMP-2 (tissue inhibitor of metalloproteases-2), which inhibits certain MMPs, had no effect on the micro-perforations; TIMP-3, which inhibits some MMPs and ADAMs, also had no effect (Fig. S1E). These data indicate that multiple proteases are involved in forming and maintaining BM perforations, rather than a specific MMP or ADAM. While we cannot entirely exclude that the inhibitors could have additional effects, e.g., on growth factor activation or other functions, the similar effects of two different protease inhibitors in loss of holes, increased collagen IV, and loss of translocation all suggest that direct proteolysis of the BM is essential for the generation of perforations and BM translocation.

Immunostaining for collagen IV in BB-94 treated glands revealed enhanced accumulation and aggregation around the end buds, consistent with reversal of protease-mediated degradation of the BM. Live-organ imaging revealed that treatment of E13 SMGs with BB-94 gradually inhibited BM motion; after 12 h, the micro-perforations were substantially diminished, collagen IV increased three-fold around the end buds (Fig. 4C, S2A), and local BM distensibility was significantly reduced (Fig. 3E). Kymograph analysis of this 12-h time period revealed a two-fold reduced rate of bud outgrowth following prolonged protease inhibition (Fig. 4D, S2A). This decreased expansion was not accompanied by decreased cell proliferation as determined by EdU incorporation (Fig. 4J and K, S2C). In fact, the micro-perforations persisted after short-term inhibition of proliferation by hydroxyurea treatment (Fig. S2B), but eventually disappeared as morphogenesis halted after overnight treatment (data not shown). Because proliferation remained constant and branching decreased with the drug treatment, we found that the cells were slightly more densely packed in the end buds with more nuclei per area (Fig. 4L). Additionally, global translocation of the BM rearward stopped after 12 h of BB-94 treatment; the BM actually moved forward slightly at a reduced rate compared to overall bud outgrowth (Fig. 3C; Movie S3). Together, these findings suggest that the BM requires the flexibility provided by the micro-perforations for two reasons: to allow expansion of the end buds and to allow the cells to remodel and translocate the BM.

Actomyosin contractility and protease activity function cooperatively in forming and maintaining BM perforations

Myosin II inhibition also halted the translocation of the BM (Fig. 3C; Movie S3) in addition to blocking the local distortions of the micro-perforations and tugging at the BM at the tip of the bud (Fig. 3D and E), suggesting that myosin II provides the mechanical force for both local and global matrix dynamics. We also examined

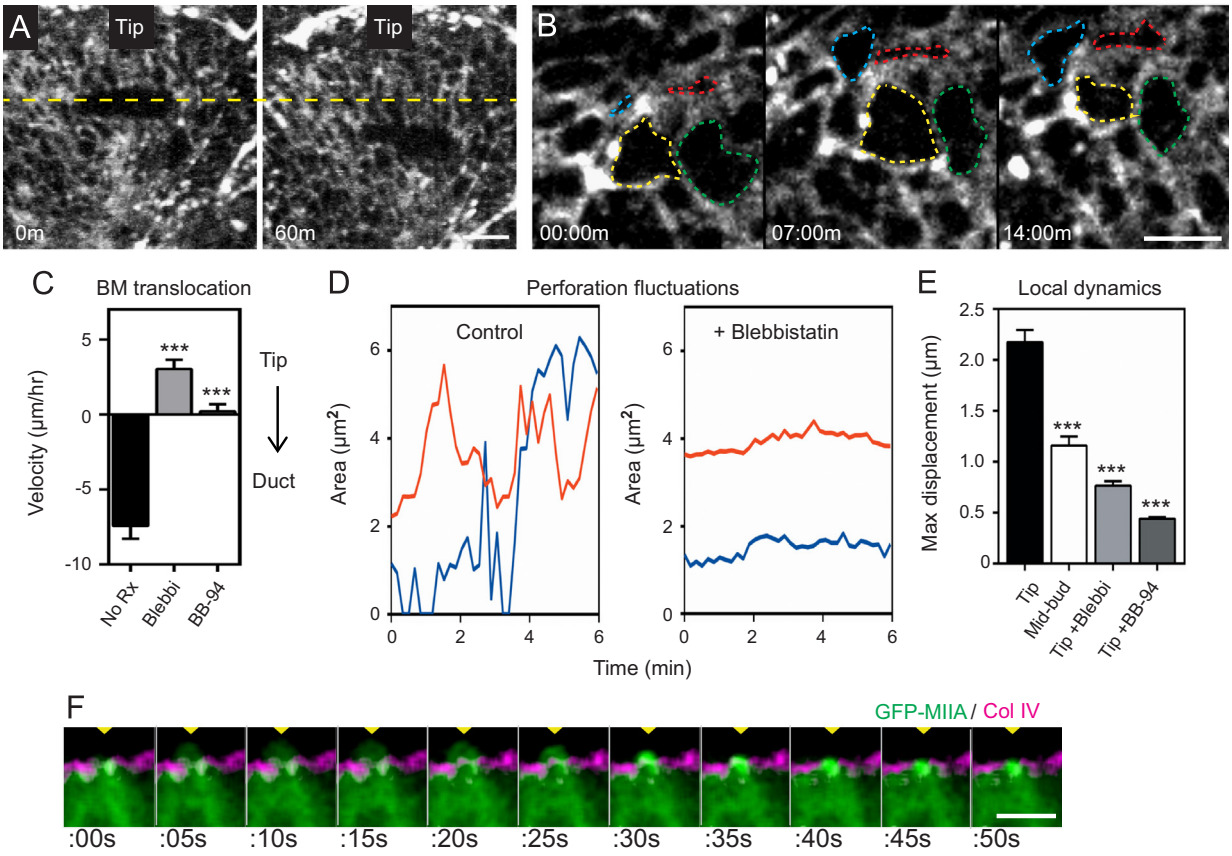

Fig. 3. Global and local basement membrane dynamics. (A) Rearward translocation of the BM as shown by the movement of a photobleached region rearward in 60 min. The dashed line indicates the starting point of the photobleached region. Scale bar: 10 μm. (B) Tracking of four (color-coded) perforations over 14 min in an E13 SMG; scale bar is 5 μm. (C) Average BM translocation velocity (±SEM) in glands with no treatment or treated with 50 μM blebbistatin or 5 μM BB-94 overnight, $^{***}p < 0.001$. (D) Change in area of two example holes in control and 50 μM blebbistatin-treated glands imaged over a span of 6 min. (E) Average distensibility of the BM (±SEM) expressed as maximum displacements within a 20-min assay period comparing a region near the tip versus mid-bud, or at the tip of glands treated with 50 μM blebbistatin or 5 μM BB-94, $^{***}p < 0.001$. (F) 50-s montage of a basal epithelial cell from an E13 GFP-myosin IIA gland (green) showing a cell process protruding (yellow arrowheads) through the BM (magenta) imaged with fluorescently tagged collagen IV antibody; scale bar: 5 μm.

whether actomyosin contractility had a role in the formation and maintenance of BM micro-perforations because recent work had shown that cells can also mechanically displace BM to augment proteolytic removal for cell invasion (Hagedorn et al., 2013). We found myosin IIA, IIB, and phospho-myosin light chain to be enriched at the epithelial cell cortex adjacent to the BM (Fig. 4E–G). At E12.5, treatment with blebbistatin inhibited cleft progression and prevented micro-perforation formation (Fig. 4H and I) without decreasing cell proliferation (Fig. 4J and K, S2C). At E13.5, a similar loss of BM dynamics was accompanied by a progressive loss of perforations until absent at 4 h; another inhibitor of actomyosin contraction, Y27632, had similar inhibitory effects on the BM perforations (Fig. S1D). Blebbistatin treatment increased collagen accumulation and decreased bud expansion, though not to the same degree as protease inhibition (Fig. S2A). Combining treatment with blebbistatin and BB-94 accelerated closure of the BM holes (Fig. 4M), suggesting that the proteases and myosin II contractility function in distinct, yet cooperative, ways to maintain the micro-perforations. Consequently, both broad protease activity and myosin II-mediated mechanical force are required for generating and maintaining regional BM perforations and successful epithelial expansion, as well as for global BM translocation.

In summary, we describe how dramatic local and global dynamics of the BM are required during development of the SMG (Fig. 5). Our study was able to document the presence of numerous micro-perforations at the bud tip by combining single-plane confocal optical slices into maximum-intensity projections to visualize the BM as a whole, rather than as tissue cross-sections. These micro-perforations are extremely dynamic and associated with increased distensibility of the BM at sites of rapid epithelial expansion. The local and global BM dynamics halt after broad protease or myosin II inhibition, suggesting that proteases increase matrix distensibility, allowing cells to physically pull and remodel it through actomyosin contractility. We speculate that general protease activity weakens the BM at the tip of the bud, and then dynamic protrusions from the underlying epithelial cells can punch through the BM, and then finally myosin II-mediated pulling of the BM stretches and elongates the perforations as the BM is translocated. We also documented global rearward BM translocation and its accumulation in dense aggregates to contribute to stabilizing and sculpting the secondary duct. We conclude that both broad protease activity and myosin II contractility work together to form and maintain the micro-perforations, to sustain local and global dynamics of the BM, and to permit effective branching morphogenesis.

Acknowledgements

We are grateful to the Adelstein laboratory for the GFP-myosin II knock-in mice. We also thank members of the Yamada laboratory for advice and W. Daley, B. DuChez and M. Hoffman for critical

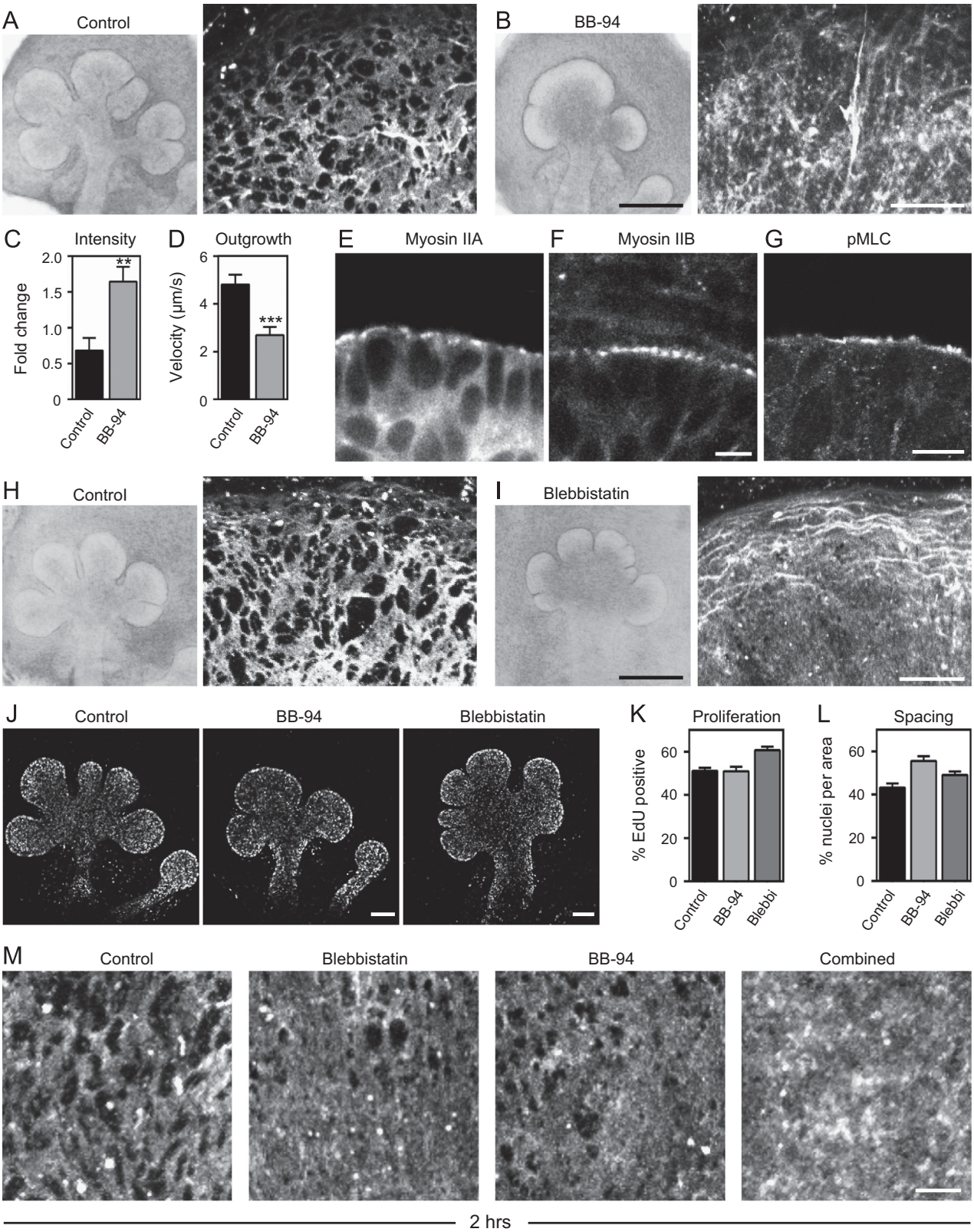

Fig. 4. Both protease and myosin II activity are required for basement membrane dynamics. (A) Control and (B) 5 μM BB-94 treated E12.5 glands immunostained with collagen IV after 24 h. Brightfield scale bar: 200 μm and collagen IV scale bar: 10 μm. (C) Fold change in BM intensity (± SEM) after 12 h of treatment with BB-94 compared with control in E13 SMGs. (D) Average bud outgrowth velocity (± SEM) after 12 h of treatment with BB-94, $^{**}p < 0.01$ and $^{***}p < 0.001$. (E) GFP-myosin IIA and (F) IIB localization in an E13 SMG dissected from knock-in mice. Scale bar: 10 μm. (G) Phospho-myosin light chain staining in an E12.5 epithelial rudiment cultured for 48 h in laminin gel. Scale bar: 10 μm. (H) Control and (I) 50 μM blebbistatin-treated E12.5 glands after 24 h. Brightfield scale bar: 200 μm and collagen IV scale bar: 10 μm. (J) E12.5 SMGs incubated overnight with or without 5 μM BB-94 or 50 μM blebbistatin and then incubated with EdU for 2 h. Scale bars: 100 μm. (K) Quantification of percent EdU positive nuclei in control and 5 μM BB-94 or 50 μM blebbistatin treated glands. (L) Quantification of percent DAPI per fixed area in control and 5 μM BB-94 or 50 μM blebbistatin treated glands. (M) E13 SMG stained for collagen IV after 2 h treatment with 50 μM blebbistatin, 5 μM BB-94, or both drugs together compared to control; scale bar: 5 μm.

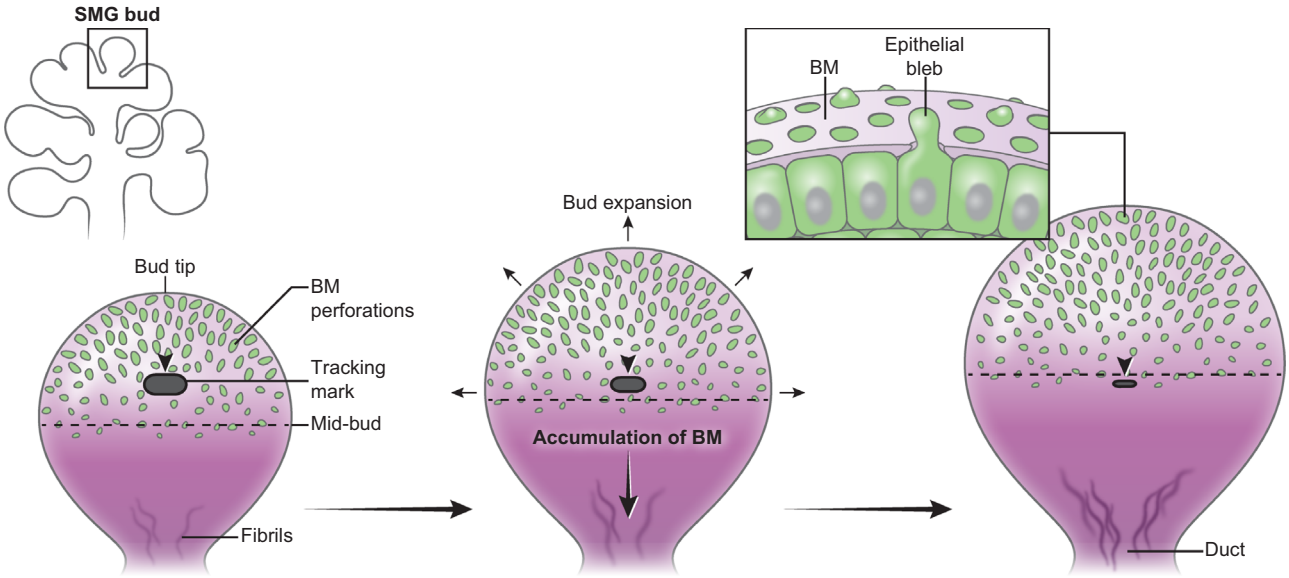

Fig. 5. Summary model. The basement membrane, displayed in magenta, surrounds the tips of expanding salivary gland epithelial end buds, and it becomes perforated with numerous holes that decrease in size and number closer to the middle of the bud. These micro-perforations are likely formed by a combination of proteases degrading the BM, epithelial cell protrusions extending through the BM (shown in green), as well as both local and global myosin II-mediated contraction of the BM. The presence of the micro-perforations increases the distensibility of the BM, allowing for outgrowth of the epithelium and myosin II-mediated rearward translocation and accumulation of the BM. Protease activity and actomyosin contractility are required for the local and global remodeling of the BM during development of the salivary gland.

reading of the manuscript. This work was supported by the Intramural Research Program of the NIH, NIDCR.

Appendix A. Supporting information

Supplementary data associated with this article can be found in the online version at http://dx.doi.org/10.1016/j.ydbio.2014.08.014.

References

Andrew, D.J., Ewald, A.J., 2010. Morphogenesis of epithelial tubes: insights into tube formation, elongation, and elaboration. Dev. Biol. 341, 34–55.
Banerjee, S.D., Cohn, R.H., Bernfield, M.R., 1977. Basal lamina of embryonic salivary epithelia. Production by the epithelium and role in maintaining lobular morphology. J. Cell Biol. 73, 445–463.
Bernfield, M., Banerjee, S.D., 1982. The turnover of basal lamina glycosaminoglycan correlates with epithelial morphogenesis. Dev. Biol. 90, 291–305.
Bluemink, J.G., Van Maurik, P., Lawson, K.A., 1976. Intimate cell contacts at the epithelial/mesenchymal interface in embryonic mouse lung. J. Ultrastruct. Res. 55, 257–270.
Candiello, J., Cole, G.J., Halfter, W., 2010. Age-dependent changes in the structure, composition and biophysical properties of a human basement membrane. Matrix Biol. 29, 402–410.
Cutler, L.S., Chaudhry, A.P., 1973. Intercellular contacts at the epithelial-mesenchymal interface during the prenatal development of the rat submandibular gland. Dev. Biol. 33, 229–240.
Daley, W.P., Yamada, K.M., 2013. ECM-modulated cellular dynamics as a driving force for tissue morphogenesis. Curr. Opin. Genet. Dev 23, 408–414.
Fata, J.E., Werb, Z., Bissell, M.J., 2004. Regulation of mammary gland branching morphogenesis by the extracellular matrix and its remodeling enzymes. Breast Cancer Res. 6, 1–11.
Fischer, R.S., Gardel, M., Ma, X., Adelstein, R.S., Waterman, C.M., 2009. Local cortical tension by myosin II guides 3D endothelial cell branching. Curr. Biol. 19, 260–265.
Fukuda, Y., Masuda, Y., Kishi, J., Hashimoto, Y., Hayakawa, T., Nogawa, H., Nakanishi, Y., 1988. The role of interstitial collagens in cleft formation of mouse embryonic submandibular gland during initial branching. Development 103, 259–267.
Grobstein, C., Cohen, J., 1965. Collagenase: effect on the morphogenesis of embryonic salivary epithelium in vitro. Science 150, 626–628.
Hagedorn, E.J., Ziel, J.W., Morrissey, M.A., Linden, L.M., Wang, Z., Chi, Q., Johnson, S. A., Sherwood, D.R., 2013. The netrin receptor DCC focuses invadopodia-driven basement membrane transmigration in vivo. J. Cell Biol. 201, 903–913.
Haigo, S.L., Bilder, D., 2011. Global tissue revolutions in a morphogenetic movement controlling elongation. Science 331, 1071–1074.
Halfter, W., Candiello, J., Hu, H., Zhang, P., Schreiber, E., Balasubramani, M., 2013. Protein composition and biomechanical properties of in vivo-derived basement membranes. Cell Adh. Migr. 7, 64–71.
Hohenester, E., Yurchenco, P.D., 2013. Laminins in basement membrane assembly. Cell Adh. Migr. 7, 56–63.
Hsu, J.C., Koo, H., Harunaga, J.S., Matsumoto, K., Doyle, A.D., Yamada, K.M., 2013. Region-specific epithelial cell dynamics during branching morphogenesis. Dev. Dyn. 242, 1066–1077.
Ihara, S., Hagedorn, E.J., Morrissey, M.A., Chi, Q., Motegi, F., Kramer, J.M., Sherwood, D.R., 2011. Basement membrane sliding and targeted adhesion remodels tissue boundaries during uterine-vulval attachment in *Caenorhabditis elegans*. Nat. Cell Biol. 13, 641–651.
Kelley, L.C., Lohmer, L.L., Hagedorn, E.J., Sherwood, D.R., 2014. Traversing the basement membrane in vivo: a diversity of strategies. J. Cell Biol. 204, 291–302.
Kim, H.Y., Nelson, C.M., 2012. Extracellular matrix and cytoskeletal dynamics during branching morphogenesis. Organogenesis 8, 56–64.
Larsen, M., Wei, C., Yamada, K.M., 2006. Cell and fibronectin dynamics during branching morphogenesis. J. Cell Sci. 119, 3376–3384.
Lehtonen, E., 1975. Epithelio-mesenchymal interface during mouse kidney tubule induction in vivo. J. Embryol. Exp. Morphol. 34, 695–705.
McKee, K.K., Harrison, D., Capizzi, S., Yurchenco, P.D., 2007. Role of laminin terminal globular domains in basement membrane assembly. J. Biol. Chem. 282, 21437–21447.
Mollard, R., Dziadek, M., 1998. A correlation between epithelial proliferation rates, basement membrane component localization patterns, and morphogenetic potential in the embryonic mouse lung. Am. J. Respir. Cell Mol. Biol. 19, 71–82.
Moore, K.A., Polte, T., Huang, S., Shi, B., Alsberg, E., Sunday, M.E., Ingber, D.E., 2005. Control of basement membrane remodeling and epithelial branching morphogenesis in embryonic lung by Rho and cytoskeletal tension. Dev. Dyn. 232, 268–281.
Nakanishi, Y., Sugiura, F., Kishi, J., Hayakawa, T., 1986. Collagenase inhibitor stimulates cleft formation during early morphogenesis of mouse salivary gland. Dev. Biol. 113, 201–206.
Patel, V.N., Rebustini, I.T., Hoffman, M.P., 2006. Salivary gland branching morphogenesis. Differentiation 74, 349–364.
Pflicke, H., Sixt, M., 2009. Preformed portals facilitate dendritic cell entry into afferent lymphatic vessels. J. Exp. Med. 206, 2925–2935.
Poschl, E., Schlotzer-Schrehardt, U., Brachvogel, B., Saito, K., Ninomiya, Y., Mayer, U., 2004. Collagen IV is essential for basement membrane stability but dispensable for initiation of its assembly during early development. Development 131, 1619–1628.
Rebustini, I.T., Myers, C., Lassiter, K.S., Surmak, A., Szabova, L., Holmbeck, K., Pedchenko, V., Hudson, B.G., Hoffman, M.P., 2009. MT2-MMP-dependent release of collagen IV NC1 domains regulates submandibular gland branching morphogenesis. Dev. Cell 17, 482–493.
Rowe, R.G., Weiss, S.J., 2009. Navigating ECM barriers at the invasive front: the cancer cell-stroma interface. Annu. Rev. Cell Dev. Biol. 25, 567–595.
Rozario, T., DeSimone, D.W., 2010. The extracellular matrix in development and morphogenesis: a dynamic view. Dev. Biol. 341, 126–140.

Silberstein, G.B., Daniel, C.W., 1982. Glycosaminoglycans in the basal lamina and extracellular matrix of the developing mouse mammary duct. Dev. Biol. 90, 215–222.
Wang, H., Lacoche, S., Huang, L., Xue, B., Muthuswamy, S.K., 2013. Rotational motion during three-dimensional morphogenesis of mammary epithelial acini relates to laminin matrix assembly. Proc. Nat. Acad. Sci. U.S.A. 110, 163–168.
Wessells, N.K., Cohen, J.H., 1968. Effects of collagenase on developing epithelia in vitro: lung, ureteric bud, and pancreas. Dev. Biol. 18, 294–309.
Yurchenco, P.D., 2011. Basement membranes: cell scaffoldings and signaling platforms. Cold Spring Harbor Perspect. Biol. 3.
Zamir, E.A., Rongish, B.J., Little, C.D., 2008. The ECM moves during primitive streak formation—computation of ECM versus cellular motion. PLoS Biol. 6, e247.
Zhang, Y., Conti, M.A., Malide, D., Dong, F., Wang, A., Shmist, Y.A., Liu, C., Zerfas, P., Daniels, M.P., Chan, C.C., Kozin, E., Kachar, B., Kelley, M.J., Kopp, J.B., Adelstein, R. S., 2012. Mouse models of MYH9-related disease: mutations in nonmuscle myosin II-A. Blood 119, 238–250.